Journal of Materials Chemistry A

Flexible Thin Film Lithium Battery with Chemical Vapor Deposited Organic Complex Cathode

Journal:	*Journal of Materials Chemistry A*
Manuscript ID	TA-ART-12-2021-010867.R1
Article Type:	Paper
Date Submitted by the Author:	25-Feb-2022
Complete List of Authors:	Li, Zhuo; University of Rochester, Chemical Engineering Hu, Fei ; University of Rochester, Chemical Engineering Huo, Ni; University of Rochester, Chemical Engineering Tenhaeff, Wyatt; University of Rochester, Chemical Engineering

ARTICLE

Flexible Thin Film Lithium Battery with Chemical Vapor Deposited Organic Complex Cathode

Received 00th January 20xx,
Accepted 00th January 20xx

DOI: 10.1039/x0xx00000x

Zhuo Li,[a] Fei Hu,[a] Ni Huo,[a] and Wyatt E. Tenhaeff [a]

Organic cathode materials have attracted significant research attention recently, yet their low electronic conductivity limits their application as solid-state cathodes in lithium batteries. This work describes the development of a novel organic cathode chemistry with significant intrinsic electronic conductivity for solid-state thin film batteries. A polymeric charge transfer complex (CTC) cathode, poly(4-vinylpyridine)-iodine monochloride(P4VP·ICl), was prepared by initiated chemical vapor deposition (iCVD). Critical chemical, physical, and electrochemical properties of the CTC complex were characterized. The complex was found to have an eletronic conductivity of 4×10^{-7} S/cm and total conductivity of 2×10^{-6} S/cm at room temperature, which allows the construction of a 2.7 μm thick dense cathode. By fabricating a P4VP·ICl|LIPON|Li thin film battery, the discharge capacity of P4VP·ICl was demonstrated to be >320mAh/cm^3 on both rigid and flexible substrates. Flexible P4VP·ICl|LIPON|Li battery was prepared by simply replacing rigid substrate with flexible polyimide substrate and the as-prepared battery can be bent 180° while maintaining electrochemical performance.

Introduction

Beyond their primary application in consumer electronics and electric vehicles, lithium-ion batteries (LIBs) are essential to advanced microelectronic applications such as smart cards, sensors, wearable electronics, and microelectromechanical systems (MEMs).[1] These applications require miniaturized dimensions, mechanical flexibility, safety, and ease of packaging, in addition to good power performance and long operational life. As solid-state energy storage devices, thin film batteries not only provide high intrinsic safety but also excel in many other key aspects, such as high volumetric energy density, fast charge/discharge rate and cyclability. The schematic provided in **Figure 1a** shows the typical structure of a thin film battery. The fully dense film morphologies and lack of binder and conductive additives enables high volumetric energy, excluding the mass and volume of the substrate. The metal current collector, cathode, solid electrolyte and Li anode are deposited onto a substrate by a sequence of deposition processes, and the total thickness of thin film battery is only several micrometers.[2] For a typical thin-film battery with an intercalation cathode, a layer of amorphous material such as $LiCoO_2$ (LCO) or $LiMn_2O_4$ (LMO) is deposited onto a metalized substrate by radiofrequency (RF) sputtering and then annealed to crystallize into the optimal crystalline microstrcuture.[3,4] Subsequently, the solid state electrolyte, lithium phosphorus oxynitride (LIPON), is deposited directly onto the cathode. Its decent lithium ion conductivity (10^{-6} S/cm), extremely low electronic conductivity (on the order of 10^{-14} S/cm), wide electrochemical stability, and large elastic modulus enables stable cycling of Li metal anodes.[5, 6] Finally, Li metal is evaporated onto the solid electrode layer to create the anode. Thin film batteries are a prime example of highly reversible charge/discharge in solid-state Li metal batteries.[2]

However, thin film battery with intercalation cathode is still limited in several important factors, especially processing speed and scalability. First, preparation of both the cathode and the electrolyte material are most frequently done by RF sputtering.[4] Deposition rate of dielectrics by RF sputtering is considerably slower than for conductive materials.[7] Since thickness of practical thin film batteries are usually several micrometers, the throughput of RF sputtering is a significant limitation. Second, the utilization of intercalation cathodes constrains the substrate composition since high temperature annealing is required to generate the desired microstructure. Typical substrates include alumina, quartz, and silicon wafers. This high temperature thermal annealing excludes most flexible thermoplastic materials as potential low-cost alternative substrates. An indirect approach of preparing flexible thin film battery has been demonstrated by Koo *et al*, where the cell is first deposited on mica and transported to PDMS as a flexible support.[8] While the electrochemical performance is preserved, the processing is very delicate and not readily scaled-up. Finally, recrystallization of sputtered electrolyte results in microstructural orientation (texturing) due to thermal stresses, which also leads to rough surface topographies and film fracture.[9] Compensating the increased surface roughness and defects requires thicker solid electrolyte layer (LIPON), which further reduces the throughput by increasing the required deposition durations.

[a] *Department of Chemical Engineering, University of Rochester, Rochester, New York 14627， United States.*

† Footnotes relating to the title and/or authors should appear here.
Electronic Supplementary Information (ESI) available: [details of any supplementary information available should be included here]. See DOI: 10.1039/x0xx00000x

To address these intrinsic challenges associated with intercalation cathodes, novel cathode chemistries are needed with comparable energy storage performance. Solid, amorphous thin film cathodes are expected to significantly increase processing throughput, reduce cost, and enable flexible polymeric substrates by eliminating the thermal annealing step. Many novel cathode chemistries have been developed for solid state batteries, such as organic and conversion type cathodes (halogen, halide, sulfur *etc*).[10, 11] Among them, organic cathodes are attractive due to their sustainability and considerable cost advantage over intercalation materials.[12, 13] When cast as a composite cathode (consisting of organic active material, conductive additive, and polymeric binder) and employed in a conventional lithium ion cell with liquid electrolyte, organic cathodes can deliver high specific capacity/energy and acceptable cyclability. [13] Yet solid-state organic batteries are limited by the very low electronic conductivity of the organic active material. In conventional lithium ion cells, the problem is circumvented by adding large amounts of conductive additive (>30%) to the composite cathode.[12, 13] In dense, solid-state electrolytes without additional conductive additive, it was found that approximately only the first 10 nm of the cathode layer is electrochemically active, regardless of the deposited thickness.[14] By comparison, thin film cathodes are usually >1µm thick; ideally, they are deposited as thick as possible since the cathode volume defines the overall energy density of the cell.[15] To achieve comparable areal specific capacity with layered oxide thin film batteries, electronic conductivity of the organic cathode must be increased.

This work is aimed at providing a possible solution to these challenges by constructing a thin-film system with a novel organic cathode material. Two objectives are expected to be achieved in the work: (1) identify an amorphous solid cathode material that allows non-PVD deposition to increase the throughput of cathode preparation and allow wider processing capabilities and (2) reduce the required thickness of LIPON electrolyte by introducing an isotropic, amorphous cathode, which further lowers the manufacturing time and cost. Initiated chemical vapor deposition (iCVD) was chosen as a fast deposition method. Among various methods of depositing organic polymeric films, iCVD has several important advantages, such as high deposition rates, broad compositional versatility and tunability, deposition conformality and processing simplicity.[16] A schematic of iCVD used in this work is shown in **Figure 1b**. During iCVD process, initiator vapors pass over a heated filament, generating gas-phase radicals. Monomer vapor and initiator radicals are then adsorbed onto the substrate and polymerizes on the surface. Since the polymerization proceeds in the adsorbed phase, deposition of polymer is conformal.[17] In comparison, RF sputtering is slow and typically line-of-sight, often resulting in non-conformal deposition on the substrate. In this work, a dense and smooth polymer film were prepared by iCVD on current collector as matrices for the electrochemically active species.

A novel strategy utilizing charge transfer complex (CTC) between halogen and basic polymer matrices was examined to solve the issue of low electronic conductivity. CTC between halogen/amine are known mixed ionic-electronic conductor (MIEC) with considerable electronic/ionic conductivity. Both the solution and neat CTC between halogen/interhalogen and pyridine are ionically and electronically conductive.[18, 19] In addition, previous studies on Li-halide battery guide the development of halogen-based CTC batteries. For example, with appropriate absorbent such as poly(vinylpyrrolidone) or carbon, I_2 can deliver >2.7 V voltage and >200 mAh/g capacity in aqueous or organic liquid electrolyte.[20-22] Solid-state lithium-I_2 battery with I^- conductor has also been been previously demonstrated. [23]

In this work, a complex of poly(4-vinyl pyridine) (P4VP) and iodine monochloride (ICl) was thoroughly explored as a CTC cathode. The polymer matrix is chosen because pyridine has relatively high basicity among organic bases (pK_a = 5.2 of conjugate acid), which allows the formation of stable CTC with halogen/interhalogen,[24] and iCVD of P4VP is an established method allowing fast and reproducible preparation of the CTC cathode.[25] ICl was chosen as the electrochemically active reagent in the CTC due to its high voltage (>3.6V, demonstrated in this work) and high theoretical specific capacity (330mAh/g). These properties make P4VP·ICl a favorable cathode material compared to Li/I_2 (2.7 V) and Li/Br_2 (3.4 V).[23, 26] In addition, the higher Lewis acidity of ICl allows it to form a stable charge transfer compound with P4VP, allowing the following vacuum deposition of LIPON.

This study describes the development of P4VP·ICl for thin film batteries. Thin film P4VP·ICl complex was prepared, and its essential properties were characterized then compared to P4VP·I_2. Flexibility of the battery was achieved by replacing quartz substrate with Kapton, a widely used polyimide material. The cyclability of P4VP·ICl system was also examined and future work with novel polymer matrices with higher oxidative stability, lower α-H activity and higher basicity is proposed.

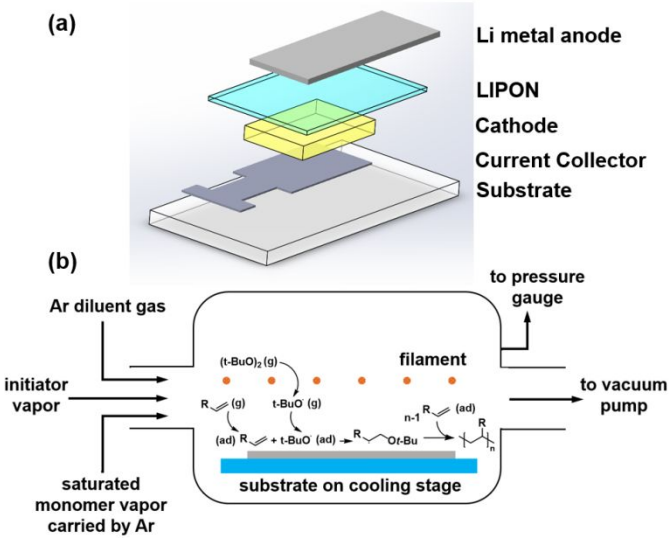

Figure 1 (a) Schematic of P4VP·ICl thin film battery fabricated in this study. (b) Schematic illustration of iCVD reactor and reactions.

Experimental Methods

Preparation of CTCs

Two CTCs, P4VP·ICl and P4VP·I_2, were prepared in bulk and as thin films. To prepare P4VP·ICl in bulk, 1 g P4VP (Scientific Polymer Products, viscosity average molecular weight = 200,000 g/mol) was dissolved in 150 mL 2-propanol (Fisher Scientific, 99%) to form a colorless solution. Then, 1.60 g ICl (1.04 eq.) was dissolved in 100mL THF (Fisher, HPLC grade), forming a red to brown solution. Be advised that solvation of ICl in THF is highly exothermic and may splatter. The ICl solution was added dropwise into strongly agitated P4VP solution, and light-yellow precipitate formed immediately. After adding ICl solution, the reaction mixture rested for 30 min. The precipitate was filtered and washed with isopropanol until the wash was colorless. The precipitate was then vacuum dried for 2 hr at room temperature and stored in desiccator. The product, P4VP·ICl is a slightly yellow powder, obtained in near theoretical yield. P4VP·I_2 is prepared with similar method, replacing ICl with I_2 (2.52 g, 1.04eq). Both P4VP·ICl and P4VP·I_2 are insoluble in THF, isopropanol, diethyl ether and dimethyl carbonate, soluble in DMF and DMSO, and react with acetone.

To prepare P4VP·ICl and P4VP·I_2 as thin film cathodes, a P4VP thin film is first deposited onto a Pt current collector. A 70 nm thick platinum layer was sputtered onto a quartz substrate (1×1×0.04 inch) using DC sputtering. For flexible thin film batteries, the quartz substrate is replaced by Pt metalized Kapton® film (McMaster-Carr, 0.05 mm thickness). The P4VP thin film was then deposited on the Pt using iCVD to fully cover the current collector area, while a small section on the edge of the substrate was masked during deposition to allow electrical connect. The effective battery area was 0.6 cm^2 (0.4×1.5cm), defined by the area of the Pt current collector pad coated by P4VP. A schematic illustration of the battery fabrication process and the definition of the active area can be found in **Figure S1**. P4VP was prepared using a custom built iCVD system employing argon carrier gas. A flow of high purity argon (5 sccm) was used to introduce 4-vinylpyridine (Fisher, 95% pure, kept at 25°C) vapor into the chamber. 2 sccm of di-*tert*-butyl peroxide (TBPO, Fisher, 99% pure) was used as initiator. Additional 10 sccm of Argon patch flow was used to dilute the precursor feed to provide better film uniformity.[27] The quartz substrate was placed on a copper stage kept at 25°C using a liquid temperature control chiller. The chamber pressure was regulated at 1000 mTorr. Thickness of the deposited film was monitored *in situ* with a laser interferometer. Typically, 1.6 µm of poly(4-vinylpyridine) was deposited onto the substrate over 100 min. The deposited P4VP thin film was kept in a desiccator overnight to prevent physical adsorption of moisture before halogen incorporation.

After deposition of the P4VP film, I_2 or ICl is incorporated into the P4VP thin film. For P4VP·I_2, I_2 was incorporated into P4VP film using solution treatment. The film is immersed in 0.08 mol/L I_2-hexanes solution overnight in argon filled glovebox (I_2: Sigma-Aldrich, >99.99% purity; hexanes: Optima, HPLC grade). After the treatment, the film is washed with neat hexanes until no I_2 color was seen in the wash. For P4VP·ICl, ICl was incorporated into P4VP film using gas phase treatment due to the low solubility of ICl in hexanes. Red lighting is essential for this step, since ICl is highly photosensitive. Common fluorescent lamp causes heterolysis of ICl and degradation of P4VP film over long period of treatment. A drop of ICl liquid is placed in a small open glass container and was sealed with P4VP sample inside a larger glass jar. The jar is left in an incubator set to 30 °C for 1h. A saturated ICl gas atmosphere is created inside the jar and ICl absorption into the polymer film was observed.

Characterization of CTCs

To determine the stoichiometry and vacuum resistance of P4VP·ICl and P4VP·I_2, 2 µm thick P4VP was deposited on pre-weighed Si wafer. The P4VP coated wafer was heated at 70 °C overnight to remove physically adsorbed monomer. The sample is weighed again with Mettler Toledo XPR6UD5 microbalance (0.5 µg accuracy). Then, ICl and I_2 were incorporated into the film. CTC samples were kept in desiccator for 24h to remove any physically adsorbed halogen before weighed again. Weighed samples were then moved to a vacuum desiccator and pumped down for 30 min. Samples were weighed again to measure the vacuum loss of halogen. Optical properties and thicknesses of P4VP·ICl films were characterized using a J. A. Wollam RC2 ellipsometer. Ellipsometric data was collected at an incident angle of 65° over the wavelength range of 210-1690 nm. Cauchy and Basis spline (B-spline) model were used to fit the transparent and absorbing region of P4VP·ICl thin films, respectively. The refractive index dispersion spectrum of each layer was derived by fitting the experimental data with the calculated model data. To confirm the structure of P4VP·ICl and P4VP·I_2, UV-Vis and FTIR spectrum was collected. For UV-Vis (ThermoScientific Evolution 300), 50 nm thick P4VP was coated on quartz substrate, and ICl/I_2 were incorporated into the film. The spectrum was collected with 1 nm interval from 190 nm to 800 nm. For FTIR spectrum, 2000 nm thick films of P4VP, P4VP·ICl and P4VP·I_2 were coated onto IR transparent Si wafer. The spectrum was collected with Thermo Scientific Nicolet iS-50 infrared spectrometer with 4cm^{-1} resolution, integrated over 32 scans. The bare Si spectrum is subtracted from the data to obtain the spectrum of the complexes. White light interferometry (Zygo NewView 600) was performed on P4VP film to confirm the surface roughness of P4VP film.

Electrochemistry

To characterize the energy storage performance of P4VP·ICl, thin-film batteries consisting of P4VP·ICl|LIPON|Li were prepared by RF sputtering and Li evaporation. First, 150 nm of LIPON is sputtered onto the cathode using radiofrequency sputtering. A Li_3PO_4 target (99.9%, Kurt J. Lesker) is sputtered under ultrahigh purity N_2 atmosphere (20 mTorr) using an RF sputtering system (80 W plasma power) with 75 nm/h deposition rate. The cathode-electrolyte stack is transported into an argon filled glovebox (H_2O<10ppm) and 1.5 µm thick Li metal anode is thermally evaporated onto the LIPON surface.

Cyclic voltammetry of P4VP·ICl was collected on P4VP·ICl|LIPON|Li cell at 70 °C with 0.5 mV/s scanning rate. The cell is scanned between 3.7 V and 2.0 V. For charge/discharge experiments, P4VP·ICl|LIPON|Li thin film battery was kept under argon atmosphere (H_2O and O_2 < 1 ppm) during testing. The cell is clamped onto a custom designed battery holder, which is thermostated during testing. The cell was discharged from OCV to 2.0V at various temperatures (37 °C, 55 °C, 70 °C) and current densities (5 µA/cm^2, 10 µA/cm^2 and 20 µA/cm^2). For characterization of reversibility, the cell is recharged at 10µA/cm^2 to 3.7V and held at 3.7V until the residual current is below 0.1 µA. A Biologic SP-300 potentiostat was used for electrochemical measurements.

Results and Discussion

Physical properties of P4VP·ICl and P4VP·I_2 charge transfer complexes

A custom iCVD chamber was employed for the deposition of P4VP films. The overall process is described in **Scheme 1**. The vapor-phase reaction mixture is introduced into the pressure-controlled deposition chamber and passes over a heated nichrome filament suspended above the substrate. Radical species are generated by thermal decomposition of TBPO. Monomer and initiator radical are adsorbed onto the temperature-controlled substrate, and radical polymerization occurs subsequently on the substrate surface to form a conformal P4VP coating.[16, 25]

The iCVD method provides fast deposition rate on the order of 15 to 20 nm/min for P4VP, and the prepared film was utilized for CTC formation without additional post-processing. While the deposition rate of iCVD polymers can easily reach 100nm/min or greater, the deposition rate was deliberately limited in this study to ensure good thickness uniformity on the battery current collectors.[16] On the other hand, sputtering of intercalation materials, such as LCO, is typically much slower (deposition rate <10 nm/min) and requires thermal annealing to crystallize into a polycrystalline microstructure.[28, 29] Surface roughness of the P4VP film was confirmed with white light interferometry (**Figure S2**). The film is smooth with root mean square roughness of 1.1 nm. In comparison, surface texture and cracks often develop in annealed intercalation cathodes due to the thermal stresses from annealing.[9] Thicker electrolyte layers are required to compensate for this roughness and fully cover the layer and prevent shorting. Given its smooth surface topography, P4VP-based cathodes should allow for thinner electrolyte layers and hence, lower electrolyte resistances.

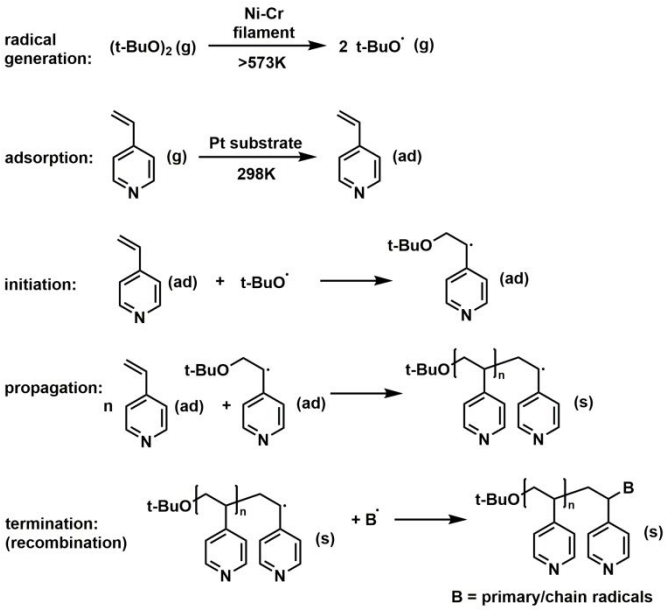

Scheme 1. Reactions in iCVD process. Multiple termination routes are possible; radical recombination is shown as an example.

To prepare the cathode material, P4VP film is further treated with halogen compounds to form charge transfer complexes. Two materials, P4VP·I_2 and P4VP·ICl were prepared. I_2 was incorporated into P4VP film by immersing the film into 0.08 M I_2-hexanes solution. Due to the larger polarity of ICl molecule, ICl has limited solubility in nonpolar hexanes; thus, gas phase incorporation was employed to prepare P4VP·ICl instead. This was achieved by simply exposing the film to saturated ICl vapor in a sealed vessel. The ICl incorporation resulted in a 154.7±7.5% increase in mass from the initial P4VP film, suggesting that a 1:1 complex between ICl and the pyridine ring formed (expected increase for a 1:1 complex [C_7H_7N·ICl] is 154.4%). For P4VP·I_2, the mass of the precursor P4VP film increased by 237.3±20.7% upon I_2 incorporation, which is also close to the expectation for a 1:1 complex [C_7H_7N·I_2] (241.4%). Digital photographs and UV-Vis spectra of the complex films are provided in **Figure S3**. The precursor P4VP film has negligible absorption in the visible range and appears colorless and transparent. P4VP·I_2 strongly absorbs UV light ($\lambda_{peak,1}$ = 251 nm) and blue light ($\lambda_{peak,2}$ = 389 nm), thus appearing dark brown to red in color. P4VP·ICl has strong, complex absorption in the UV region (220-246 nm) but only weak absorption in the visible range (>380 nm), thus appears to be slightly yellow. The color difference between P4VP·ICl and P4VP·I_2 can be explained by the polarity of the CTC compound. Interaction between iodine and electron donor is known to cause a strong blue shift of the I_2 absorption peak, thus the brown to red color of P4VP·I_2 is caused by the Py-$I^{\delta+}$-$I^{\delta-}$ polarization.[30, 31] Due to the much larger electronegativity of Cl, P4VP·ICl is more ionic, which further blue-shifts the absorbance of P4VP·ICl into the UV range,

explaining its limited color and transparency in the visible region.[32]

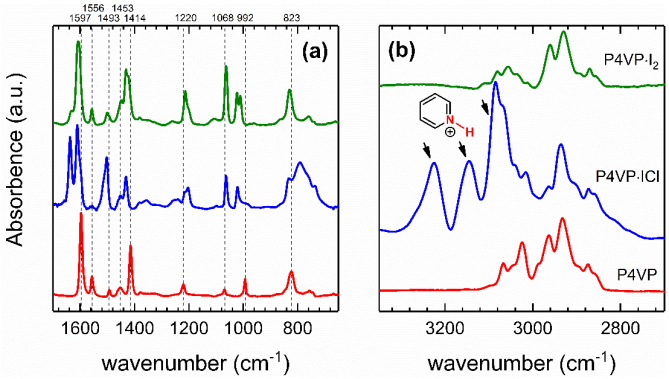

Figure 2 FTIR spectra of P4VP and its CTC complexes: (a) 1700 cm^{-1} to 650 cm^{-1}, (b) 3350 cm^{-1} to 2700 cm^{-1}.

To further understand the structure and interactions between I_2/ICl and P4VP, FTIR spectroscopy of P4VP, P4VP·I_2 and P4VP·ICl was executed (**Figure 2**). Vibrational modes of I-Cl and polarized I-I bond are found in far infrared region (<400cm^{-1}) and cannot be resolved within the mid-IR optics of the FTIR spectrometer.[33] Yet the interaction between I_2/ICl and pyridine ring can still be detected by the change in pyridine ring vibration modes (650-1700 cm^{-1}). Key vibrational modes are summarized in **Table 1**:

Table 1. Vibrational mode assignments of pyridine ring in P4VP and CTCs.

Normal modes [a)]	P4VP (cm^{-1})	P4VP·I_2 (cm^{-1})	P4VP·ICl (cm^{-1})
8a	1597	1632/1607	1637/1610
8b	1556	1556	-
19a	1493	1500	1502
CH_2 scissor	1453	1450	1452
19b	1414	1431/1423	1431
9a	1220	1213	1214/1203
12	1070	1063	1063
1	992	1023/1010	1019
11	823	830	833

a) Modes are labelled according to the Wilson notation.[39]

IR spectrum of P4VP and P4VP·I_2 are in good agreement with previous report, which confirms the formation of P4VP·I_2 complex.[35] A consistent trend of peak shifting can be observed in both P4VP·ICl and P4VP·I_2, caused by the electron redistribution to $I^{\delta+}$ center in CTCs. P4VP·ICl has a larger impact on both intensity change and peak shifting compared with P4VP·I_2. Intensity of free pyridine ring vibration (mode 8b, 1556cm^{-1}) decreases in both P4VP·I_2 and P4VP·ICl, nearly disappearing in the latter spectrum. As a stronger Lewis acid, ICl causes stronger electron redistribution from N in the pyridine ring to $I^{\delta+}$ center than I_2, which causes the pyridine ring to have a lower electron density then P4VP·I_2. Hence, the shift of the pyridine ring vibrational modes is more significant in P4VP·ICl.[36] Another notable change in **Figure 2a** is the splitting of mode 8a. The 1597 cm^{-1} P4VP 8a mode becomes two peaks, which correspond to the CTC and protonated pyridinium ring.[37] In P4VP·ICl, the 1597 cm^{-1} peak splits to 1610 cm^{-1} (R-Py·ICl) and 1637 cm^{-1} (pyridinium). In P4VP·I_2, the 1597 cm^{-1} peak splits to 1607 cm^{-1} (R-Py·I_2) and 1632 cm^{-1} (pyridinium), while the relative intensity of pyridinium peak is significantly lower than in the corresponding P4VP·ICl. The higher wavenumber pyridinium peak suggests two important facts: (1) hydrogen halide species are generated during the incorporation and (2) hydrogen halide formation during the ICl incorporation is much more prominent. Evidence of the formation of protonated pyridinium is also found in the 2700~3350 cm^{-1} region (**Figure 2b**). Most of the peaks remain unchanged in P4VP and CTCs, yet three strong new peaks are found in the P4VP·ICl complex. The additional peaks (>3067cm^{-1}) are in agreement with the FTIR spectrum of Py·HCl, which correspond to the pyridinium N^+-H vibration modes.[37-39] Formation of hydrogen halides in pyridine-halogen system *via* α-H substitution has been reported before, and is explained in **Scheme 2**.[40]

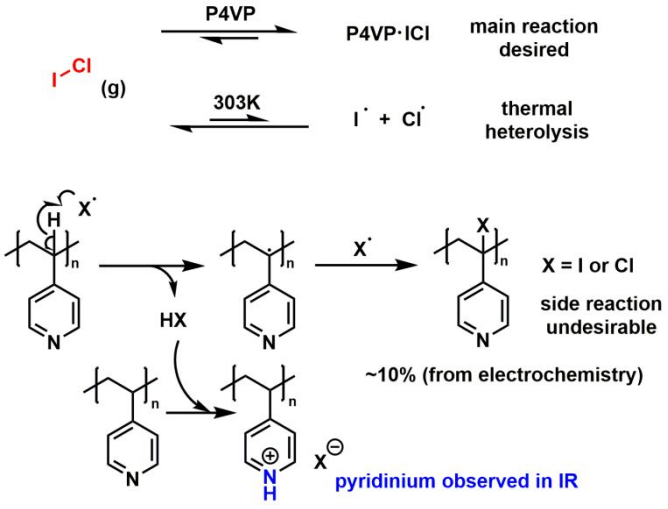

Scheme 2 Proposed reactions between P4VP and ICl during gas phase incorporation. Thermal heterolysis of ICl may result in α-H substitution in P4VP and further generate pyridinium, which is detected by FTIR.

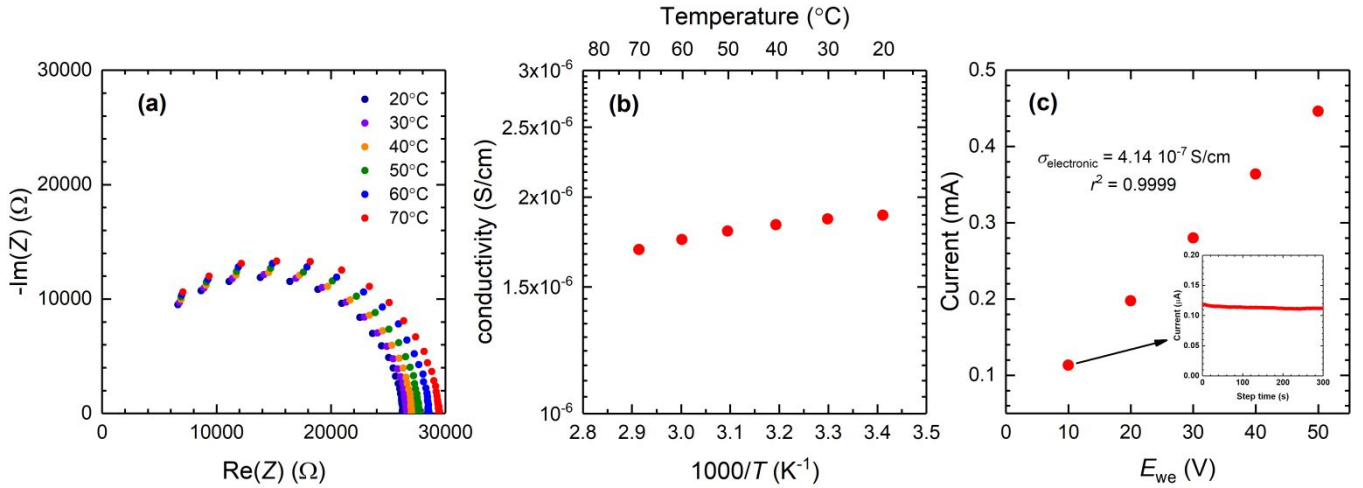

Figure 3 Electrical characterization of P4VP·ICl. (a) EIS of Pt|P4VP·ICl|Pt pellet; (b) total conductivity of the sample as a function of tempreature; (c) *I-E* relation of Pt|P4VP·ICl|Pt biased by 10mV, 20mV, 30mV, 40mV, 50mV at room temperature (25°C). Inlet: chronoamperogram of Pt|P4VP·ICl|Pt at 10mV.

A parasitic α-H substitution reaction on polymer chain may occur due to the existence of halogen radical in the system. Gas phase ICl is a rather unstable compound, with formation Gibbs free energy of only -5.8 kJ/mol (303 K), and likely generates highly active Cl radical in gas phase.[41] A fraction of the active pyridyl α-H is radically substituted and iodinated/chlorinated P4VP is formed. Hydrogen halides are formed in this process, hence protonated pyridinium was found in the spectrum. C-Cl stretch vibration (791 cm^{-1}) of the chlorinated P4VP was found in the P4VP·ICl film but not in P4VP·I_2 film (**Figure 2a)**, which further confirms that the α-H substitution can occur during CTC formation. In comparison, the iodine radical generated from I_2 homolysis is much less active, hence less HI is formed in the process.[42] As a result, the intensity of protonated pyridinium peak in P4VP·I_2 peak is smaller than P4VP·ICl. It should be acknowledged that that α-H substitution is not the only possible source of pyridinium in P4VP·ICl film. ICl may react with residual moisture to form HCl, which is then absorbed by P4VP and can react further to form pyridinium that is detected by FTIR. Yet this reaction does not result in the formation of C-Cl, which were detected spectroscopically and electrochemically (**Figure 4**), so the reaction cannot account for all of the pyridinium present in the film.

The mixed conductivity of P4VP·ICl was confirmed by measuring its conductivity using a metallized pellet. **Figure 3a** shows the electrochemical impedance spectrum of the Pt|P4VP·ICl|Pt pellet. A mixed ionic-electronic conductor (MIEC) behavior, which can be roughly described as the combination of a Warburg element and an (RC) element (the low frequency 45° straight line is not shown in the spectrum due to frequency limit of the instrument) was observed. The detailed fitting of MIEC impedance to resolve ionic and electronic transport, however, is complicated.[43, 44] In pyridine-ICl solution, many ionic conductors such as Py_2I^+, Cl^- and ICl_2^- were observed, and their concentration are linked by multiple chemical equilibria.[36] In P4VP·ICl system, the relation between ionic charge carriers is further complicated due to the existence of the polymer chain. Additionally, fitting of the MIEC impedance requires the knowledge of various microscopic properties of the material, such as diffusion coefficient of the involved species. Yet the total conductivity can be assessed using the impedance spectrum and is presented in **Figure 3b**. From 20°C to 70°C, the total conductivity of the P4VP·ICl film slightly decreases from 1.9×10^{-6} S/cm to 1.7×10^{-6} S/cm. The total conductivity follows Arrhenius behavior (r^2 = 0.99), with a low negative activation energy (-1.84 kJ/mol or -0.02 eV). This low negative activation energy is rarely seen in polymeric materials. Electronic conductivity of conjugated polymer semiconductors, such as polyacetylene, increases with temperature.[52] Likewise, the ionic conductivity of polymer-based lithium ion conductors, such as PEO-Li salt mixtures, also increases with temperature.[53] However, charge transport in P4VP·ICl is not a simple combination of these two conduction mechanisms. The conductivity of the complex is directly correlated to the coordination-dissociation equilibrium of halogen in P4VP·ICl. The electrical conductivity is determined by the molecular halogen species (I_2 or ICl), as demonstrated by the strong dependence of the electronic conductivity of P4VP·I_2 on the concentration of I_2.[54] On the other hand, ionic conductivity is contributed by the dissociated halogen ions (PyI^+, I^-, Cl^-, ICl_2^- *etc.*), which is in equilibrium with molecular halogen and each other. These equilibria are well known in pyridine-halogen liquid solution system.[36] As a result, the temperature dependence of the conductivity of P4VP·ICl will be a strong function of the speciation of the halogens due to these multiple equilibria in the polymer film. Elucidation of the exact equilibria was beyond the scope of this project, but it is reasonable to expect that conductivity will decrease with temperature if the equilibria favors species with lower diffusivities. The electronic conductivity of P4VP|ICl was measured using chronoamperometry.[45] Pt|P4VP·ICl|Pt pellet was biased from 10mV to 50mV, and the stable current was found to follow Ohm's law (r^2 = 0.9999, **Figure 3c**). From this result, P4VP·ICl appears to be semiconducting, with σ_{elec} = 4.14×10^{-7} S/cm or 22% of the total conductivity at room temperature. The conductive nature allows us to build relatively thick cathode. In

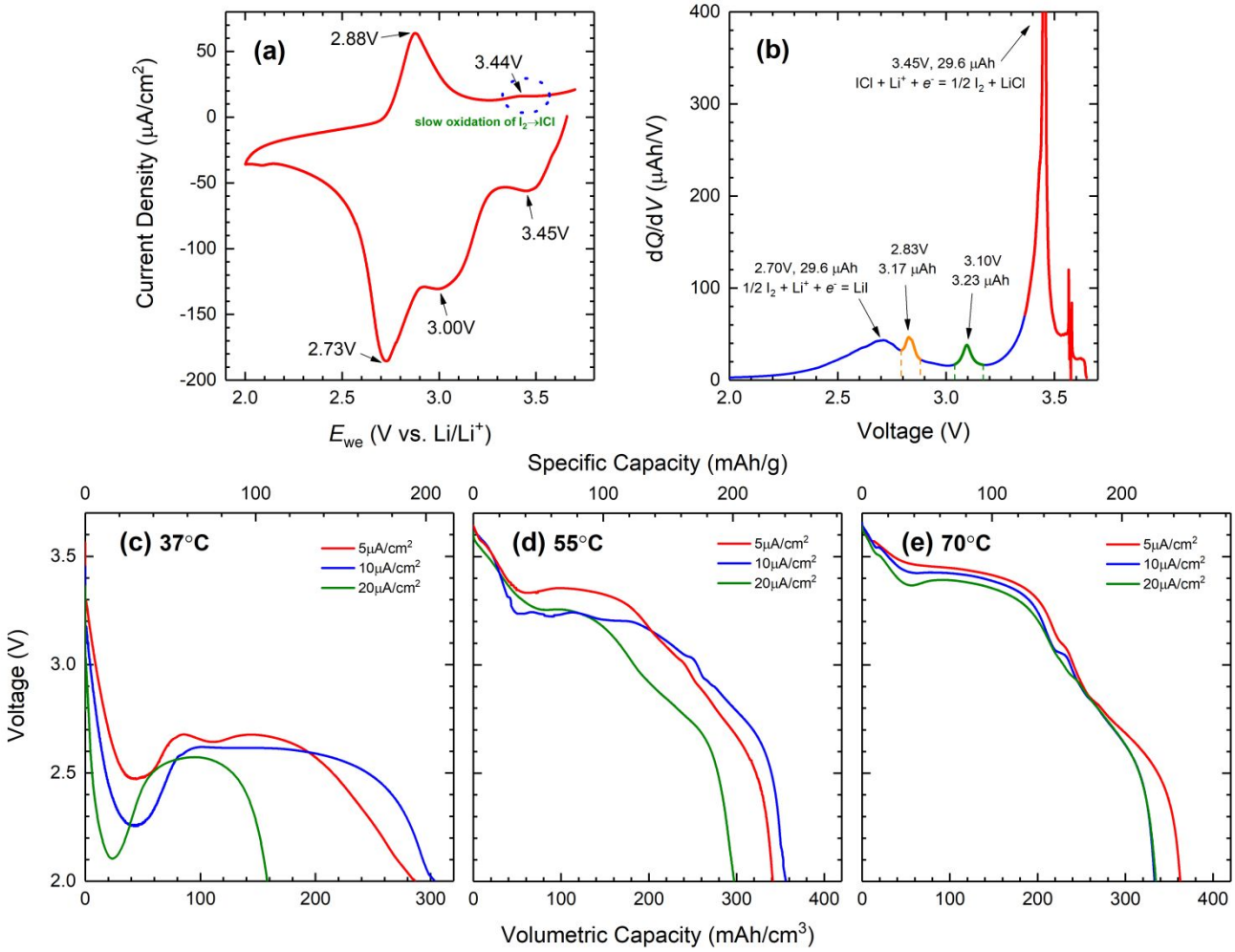

Figure 4 (a) Cyclic voltammogram of P4VP·ICl at 70 °C and 0.5mV/s scan rate. (b) d*Q*/d*V* plot of 2700nm P4VP·ICl discharge at 70°C. (c)-(e): 1st discharge profile of 2700nm P4VP·ICl-LiPON-Li thin film battery. The cell was held at (c) 37°C (d) 55 °C and (e) 70°C. Discharge current densities of 5μA/cm², 10μA/cm² and 20μA/cm² were applied.

this work, 2.7μm thick P4VP·ICl cathode were employed. In comparison, P4VP·I_2 only shows σ_{elec} = 3.6×10^{-9} S/cm at room temperature, which significantly limits the electron transport in the cathode film. It is worth noting that the conductivity of the electron donor-halogen system is governed by the amount of halogen incorporation. In this work, P4VP·I_2 and P4VP·ICl sample are vacuum dried to remove the solvent before being pressed into pellet. As a result, the molar ratio between P4VP and halogen in the pellet is slightly >1. The measured conductivities is lower than previously reported values, which are usually measured for complexes rich in halogens, where the molar ratio of polymer: halogen << 1.[46]

Since the CTC cathode is inevitability exposed to high vacuum during LIPON deposition required for fabrication of thin film batteries, the physical stability of the CTC in vacuum, i.e., vacuum resistance, is required for reproducible handling of the material and to achieve high discharge capacities. P4VP·ICl shows significantly higher vacuum resistance compared to P4VP·I_2, and good reproducibility over multiple P4VP·ICl samples was observed. This phenomenon can be explained by the thermodynamics of the reaction, P4VP·X_2 ⇌P4VP + X_2 (X_2 = I_2 or ICl). It was assumed that thermodynamics are analogous to the formation of small molecule CTC with pyridine, Py·X_2⇌Py + X_2, where the equilibrium constants are 1×10^{-3} mol/L for Py·I_2 and 2×10^{-6} mol/L for Py·ICl at standard state.[36] Hence, it is expected that the concentration of halogen molecules will be higher in P4VP·I_2 than P4VP·ICl, which evaporate from the film during vacuum processing. Experiments revealed that P4VP·I_2 lost 38% of the incorporated I_2 after 30 min of high vacuum exposure, while P4VP·ICl only lost 8% of the incorporated ICl. Another potential concern associated with the vacuum loss of halogen during LIPON deposition is the formation of a concentration gradient, which will increase the interfacial charge transfer resistance, adding to voltage losses during operating of the thin film battery. To understand this potential issue, a 2.5 μm thick P4VP·ICl film was characterized ellipsometrically before and after 30 minutes of exposure to vacuum (approx. 10^{-5} Torr). The refractive index of P4VP·ICl is a function of the ICl concentration with its high molar refractivity, which allows the distribution of ICl to be characterized indirectly through the development of an optical model of the film. A basic model with a single refractive index for the entire film represents an isotropic film with a uniform distribution of ICl. On the other hand, to model a gradient in ICl, the graded model divides the film into multiple layers of equal thickness and allows the refractive index to vary between each layer. Two

refractive index dispersion curves were obtained, representing the refractive index of the top layer at the air-film interface and the bottom layer in contact with the substrate. The initial refractive index of a P4VP film is approximately 1.58 and increases significantly upon incorporation of ICl. Specifically, when the polymer film is modelled with a gradient index (indicative of depletion of ICl from the air-film interface), the refractive index of the top layer at 632.8nm is 1.7449, while the bottom layer has a refractive index of 1.7578. The refractive index differences at these two interfaces is 0.0129, indicating a negligible concentration gradient from top to bottom. Moreover, these indexes are close to the refractive index obtained using an isotropic model (1.7495), which further suggests that a negligible gradient develops. The fit quality of these two models is quantified by the mean square error (MSE), which represents the difference between the model and the experimental data. The MSE of models was optimized using a Levenberg-Marquardt regression algorithm. The minimized MSE values of the isotropic and graded model are 17.008 and 16.812, respectively, which are both reasonably small for a 2.5 μm film. The negligible difference in MSE of 0.196 suggests that grading did not improve quality of the fit, despite the many additional fit parameters. Thus, it could not be concluded that a permanent concentration gradient develops upon exposure to vacuum. Given the thinness of the polymer film, equilibration of the ICl concentration within the film occurs reasonably fast – over a much shorter timescale than further processing and thin film battery operation. Regarding its higher conductivity, higher vacuum resistance and fast diffusion of ICl in P4VP matrices, P4VP·ICl was selected as candidate material for organic cathode thin-film battery.

Electrochemistry of P4VP·ICl

To test the electrochemical properties of P4VP·ICl cathode, LIPON and Li metal was deposited on the cathode to make a thin film battery. Schematic illustration of the sequential deposition is shown in **Figure S1**, and the structure of the stack is presented in **Figure 1a**. Due to the low surface roughness of the cathode film, it was found that 150 nm of LIPON is sufficient to completely encapsulate the cathode and reliably separate the two electrodes. A colorless LIPON layer can be seen on the uncoated part of the substrate, and the coated P4VP·ICl complex cathode maintains its slight yellow color. In comparison, the color of P4VP·I_2 becomes much lighter after the deposition due to vacuum loss of I_2. Li metal anode is applied to the cathode/electrolyte stack by thermally evaporating Li metal. The anode also serves as current collector, no encapsulation was applied. The thin film battery is moved into another glovebox for testing.

Electrochemical reactions of the P4VP·ICl-Li system are revealed by cyclic voltammetry (**Figure 4a**). The system has a stable 3.65V open circuit voltage, which was found stable between samples and insensitive to temperature. Starting from OCV, the system is first scanned to 2.0V. Three peaks (3.45V, 3.0V, 2.73V vs. Li/Li^+) can be found during the scan. The 3.45V peak is assigned to the 1st stage reduction of ICl and the 2.73V peak is assigned to the 2nd stage reduction of I_2:

$$\mathbf{2P4VP{\cdot}ICl + 2Li^+ + 2e^- = P4VP + P4VP{\cdot}I_2 + 2LiCl}$$

E_{peak} = 3.45 V vs. Li/Li^+ (1)

$$\mathbf{P4VP{\cdot}I_2 + 2Li^+ + 2e^- = 2LiI + P4VP}$$

E_{peak} = 2.73 V vs. Li/Li^+ (2)

Overall reaction: $\mathbf{P4VP{\cdot}ICl + 2Li^+ + 2e^- = LiI + LiCl + P4VP}$ (3)

Theoretical potential of the two reaction steps can be estimated using the standard formation Gibbs free energy change of ICl(s), LiCl(s) and LiI(s) (-5.7 kJ/mol, -384.0kJ/mol and -266.2 kJ/mol, respectively).[47] Without P4VP, the first step reduction of ICl has $\Delta G^{\ominus}$ = -756.6 kJ/mol, or $\varphi^{\ominus}$ = 3.92 V and the second step reduction of I_2 has $\Delta G^{\ominus}$ = -532.4 kJ/mol, or $\varphi^{\ominus}$ = 2.77 V. In P4VP·ICl system, potential of reaction (1) is also affected by the dissociation reaction of P4VP·ICl (P4VP·ICl→P4VP + ICl, $\Delta G_1 > 0$) and the formation reaction of P4VP·I_2 (P4VP + I_2 → P4VP·I_2, $\Delta G_2 < 0$). Due to the stronger Lewis acidity of ICl compared with I_2, free energy released by P4VP·I_2 formation cannot compensate the dissociation of P4VP·ICl ($|\Delta G_1| > |\Delta G_2|$), thus the peak potential is reduced to 3.45 V. Similarly, the potential of reaction (2) is affected by dissociation of P4VP·I_2, which reduces the peak potential from 2.77 V to 2.73 V.

The 2.73 V potential assigned to I_2 → LiI is in agreement with previous reports on electrochemistry of Li/I_2.[48] Thus the 3.45 V and 2.73 V peaks can be attributed to Equations (1) and (2), respectively. The 2-stage reduction of P4VP·ICl is further supported by the d*Q*/d*V* plot of the 1st discharge at 70 °C **(Figure 4b**). Four peaks can be found in the d*Q*/d*V* plot, with peak potential of 3.45 V, 3.10 V, 2.83 V and 2.70 V vs. Li/Li^+, respectively. The peak potential of 1st stage ICl reduction and 2nd stage I_2 reduction are in good agreement with CV result. An anodic scan from 2.0 V to 3.7 V vs. Li/Li^+ was used to assess reversibility of the system. At 2.88 V vs. Li/Li^+, I^- from LiI is oxidized to I_2, showing an anodic peak. However, only a small peak of I_2 → ICl is found at 3.45 V vs. Li/Li^+, which suggests that the oxidation of I^0 to I^+ is a slow process, which will significantly restrict the recharging of the system.

Beside the reduction of P4VP·ICl and P4VP·I_2, both **Figure 4a** and **Figure 4b** suggests side reactions in the system. In the cyclic voltammogram, a single peak at 3.0 V vs. Li/Li^+ is observed. In d*Q*/d*V* plot, two peaks (2.83V and 3.10 V vs. Li/Li^+) are found between the two major peaks. The two peaks have very similar capacity (1:1.01) and contributes approximately 10% of the total capacity (6.4 μAh/59.2 μAh). Combined with spectroscopic evidence, the two peaks are attributed to the reduction of halogen substituted P4VP (2.83 V for chlorinated P4VP and 3.10 V for iodinated P4VP). Such attribution is indirectly supported by the α-H substitution mechanism (**Scheme 2**), in which the recombination between benzyl radical and halogen radical should generate 1:1 by molar of the two substituted compounds. In cyclic voltammogram, the two reduction peaks cannot be distinguished, most likely due to the similar electrode kinetics and large FWHM (full width at half maximum).[49] The 3.0 V vs. Li/Li^+ peak in voltammogram is very close to the average

of the two reaction (2.97 V vs. Li/Li$^+$), which further supports the peak assignment.

Table 2. 1st discharge performance of P4VP·ICl|LIPON|Li cell.

Temperature/ current density	5μA/cm^2	10μA/cm^2	20μA/cm^2
37 °C	286 mAh/cm^3 (193 mAh/g)	303 mAh/cm^3 (205 mAh/g)	158 mAh/cm^3 (107 mAh/g)
55 °C	341 mAh/cm^3 (230 mAh/g)	356 mAh/cm^3 (240 mAh/g)	297 mAh/cm^3 (201 mAh/g)
70 °C	362 mAh/cm^3 (245 mAh/g)	333 mAh/cm^3 (225 mAh/g)	335 mAh/cm^3 (226 mAh/g)

Understanding the electrochemistry of P4VP·ICl reduction allows further investigation of the P4VP·ICl|LIPON|Li thin film cell. The 1st discharge profiles of the of P4VP·ICl|LiPON|Li thin film battery cells is presented in **Figure 4c-4e**. Cells were discharged at rates of 5 μA/cm^2, 10 μA/cm^2 and 20 μA/cm^2 at 37 °C, 55 °C and 70 °C. The resulting specific capacity is summarized in **Table 2**. To fully discharge the cell, the discharge cut-off potential was set to 2.0 V. At 37 °C, the cell showed significant polarization, possibly due to the slow diffusion of Li$^+$ in the cathode. At a 20 μA/cm^2 current density, 1.55 V overpotential (3.65 V→2.10 V) was observed, which correspond to a total cell resistance of 7.8×10^4 Ω. Similarly, total cell resistances at 5 μA/cm^2 and 10 μA/cm^2 were 1.4×10^5 Ω and 2.4×10^5 Ω, respectively. The total resistance is much larger than the combination of cathode and electrolyte (250 Ω for P4VP·ICl cathode and 225 Ω for LIPON electrolyte at 37 °C), which suggests the presence of large interfacial resistance. Such large interfacial resistance may relate to the difference in charge carrier species of P4VP·ICl (halogen species) and LIPON(Li$^+$). Similar behavior on polymer/inorganic interface has been reported before.[50] After the first 25% of the capacity, accumulation of LiCl improves the transport of Li$^+$ in the cathode and a stable 2.7 V plateau is observed.

The performance is significantly improved while the cell is heated to 55 °C due to reduced cell impedance (**Figure S4**). Polarization of the cell is reduced to 400mV, indicating significantly mitigated interfacial resistance. The cell impedance can be further reduced by heating to 70 °C, and the polarization is further reduced to <200 mV. Two distinctive voltage plateaus can be seen in the voltage profile, which correspond to the two-stage reduction of P4VP·ICl. The estimated total resistance from cathode and electrolyte contributes <40% of the total impedance to the cell at 70 °C, suggesting that the interfacial resistance between LIPON and P4VP·ICl cathode remains dominant. The total discharge capacity of the cell is comparable with layered oxide thin-film batteries (**Table 2**), reaching 362 mAh/cm^3 (245 mAh/g). These results show that despite the presence of large interfacial resistance, P4VP·ICl allows the construction of relative thick cathode without conductive additive.

Characterization of the reversibility of the P4VP·ICl cells is presented in **Figure 5** and **Figure S5**. After constant current-constant voltage (CCCV) charge of the discharged P4VP·ICl cell, considerable capacity was lost. The 2nd discharge shows that 50% of the initial capacity is recovered. Both the ~3.4 V ICl → I_2 + LiCl and the ~2.7 V I_2 → LiI discharge plateau were found in the 2nd discharge, while the initial polarization was found significantly larger than the 1st discharge process. As shown in **Figure 5a**, the ~3.4V ICl reduction plateau still appears in the 2nd and 3rd

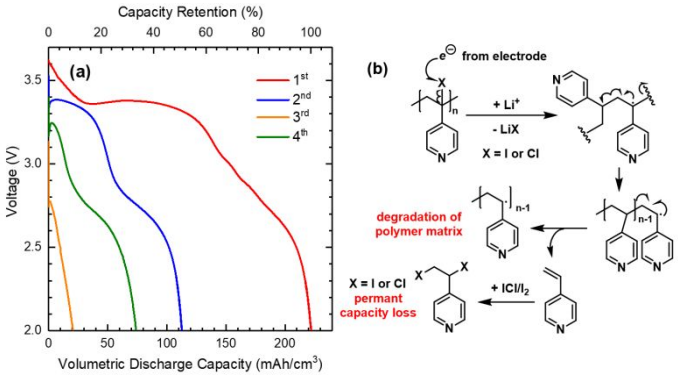

Figure 5 (a) Discharge voltage profile of P4VP·ICl|LIPON|Li cell. The cell was discharged at 10μA/cm^2 to 2.0V and recharged at 10μA/cm^2 to 3.7 V followed by a constant voltage step at 3.7V at 70°C. (b) Proposed degradation mechanism of halogen substituted P4VP.

discharge cycle, despite the unsatisfactory stability of P4VP against radical substitution and fast consumption of active material. The 2.7 V I_2 reduction plateau is also found in the 4th discharge cycle, while ICl reduction plateau has disappeared. This evidence suggests that the conversion of LiI to I_2 is easier than conversion of I_2 and LiCl to ICl. Similar observation was made in the cyclic voltammogram (**Figure 4a**), which shows that the kinetics of I^0 oxidation to I^+ is much slower than I^- to I^0. It is possible that the I^0 or Cl^0 radical intermediates during charge can also react with α-H of the polymer backbone to form iodinated/chlorinated P4VP, which will result in further capacity loss. Thus, it is expected that the α-H bearing P4VP·ICl system may have a poor recharge behavior.

Voltage profiles of the charge steps are included in **Figure S5**. Significant charge capacity decay was observed in the first 4 cycles. Increasing polarization of the cell was found during charge, indicating an increased cell impedance due to degradation of the polymer matrix and depletion of active material. A notable phenomenon was observed, where overpotential decreases during the galvanostatic charge. Such behavior can be explained by a varying cathode conductivity during charge. Since the electronic conductivity of the complex is directly related to the concentration of halogen (I_2 or ICl) complexed to the polymer matrix, cathode electronic conductivity is expected to increase as more X_2 forms during the anodic reaction, resulting in less polarization. Initially during recharge, the cell potential is mainly determined by polarization, but as the charge progresses and conductivity increases, the polarization will decrease and the charge potentials more closely approach the equilibrium potential of the P4VP·X_2 complex. As a result of the polymer matrix degradation, active material depletion and increasing polarization, the conversion of I_2 to ICl is increasingly inhibited over increased cycle number. The voltage plateau at 3.4V

associated with ICl formation is completely absent in the voltage profiles by the 4th discharge, further revealing the limited reversibility of this system. The reduction of iodinated/chlorinated P4VP may follow the proposed mechanism in **Figure 5b**, resulting in molecular weight reduction and impedance increase. Similar to the electrochemical reduction of other halogenated hydrocarbons, degradation of P4VP matrix starts with the formation of benzyl radical at the halogenated site.[51] The benzyl radical will cause chain severance and depolymerization of P4VP. The released 4-VP monomer will further react with ICl/I_2 generated from the oxidation of LiCl/LiI and reduce the discharge capacity. The overall effect is significant decrease in molecular weight and consumption of active material. Due to the low sample mass and strong interaction between P4VP and ICl, experimental confirmation of the P4VP molecular weight after discharge was not possible. Although significant capacity fading is observed during the recharge, it is expected that the cyclability of a polymeric charge transfer complex cathode can be significantly improved if the halogenation reaction during ICl incorporation is prevented. Since the halogenation reaction is directly related to the activity of α-H in P4VP structure, replacing the α-H with a less reactive moiety, such as a methyl or nitrile group, should significantly improve the stability of polymer during halogen incorporation process and the recharge process.

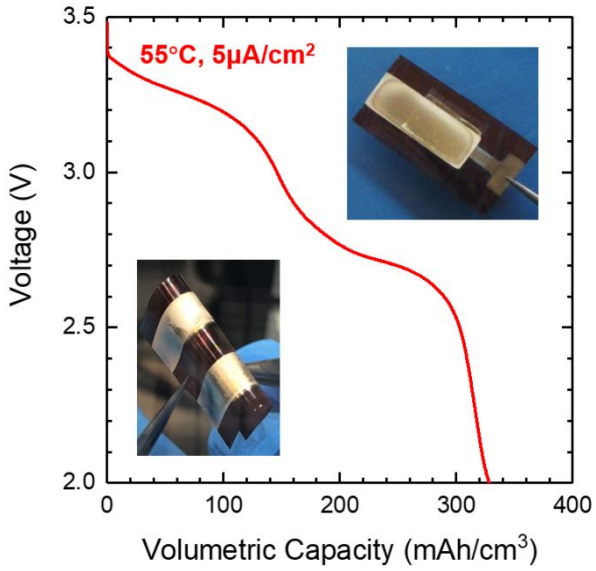

Figure 6 Discharge profile afterof flexible P4VP·ICl|LIPON|Li cell coated on Kapton® film after bending. Cell temperature was 55°C, and current density was 5μA/cm². Bottom inset: picture of a flexible thin film batteries (two batteries were deposited on this substrate). Top inset: Plan view of the battery before cycling.

Flexible Battery enabled by P4VP·ICl

Due to the advantage of the iCVD technique and P4VP·ICl gas phase incorporation chemistry, the battery can be made flexible by simply replacing conventional rigid inorganic substrates with flexible plastics without additional processing. **Figure 6** shows the performance of a flexible P4VP·ICl battery on a polyimide (Kapton) substrate. The battery can be bent 180° without compromising its electrochemical performance (discharge capacity was 328 mAh/cm³). The discharge profile of the cell shows two distinctive discharge reactions, as demonstrated in cells fabricated on quartz substrates. This evidence suggests that an iCVD-deposited, organic cathode can achieve true flexibility without any additional processing, while previous flexible battery systems, including liquid, solid-state and thin-film batteries require complete redesign of the cell. Thus, polymeric charge transfer complex cathode has considerable potential in the application of advanced Li-ion batteries.

Conclusions

P4VP·ICl charge transfer complexes have been demonstrated as a polymeric, readily processible cathode for solid state lithium thin film batteries. Smooth P4VP thin films were prepared with iCVD, and then further incorporated with ICl and I_2 to form 1:1 charge transfer complexes. With EIS and chronoamperometry, P4VP·ICl was confirmed to be both ionically and electronically conductive, with a total conductivity of 1.7×10^{-6} S/cm and electronic conductivity 4.1×10^{-7} S/cm at room temperature. The improved transport phenomenon enabled the construction of a smooth, uniform 2.7μm-thick cathode, where only 150 nm of LIPON electrolyte was needed to fully encapsulate the cathode. At elevated temperature, P4VP·ICl|LIPON|Li cell can deliver 245mAh/g specific capacity and 3.65V voltage. To the best of our knowledge, this is the first demonstration of polymer charge transfer complexes in thin-film batteries. The system showed considerable interfacial resistance, presumably due to the difference in charge carrier on P4VP·ICl and LIPON interface. Detailed spectroscopic and electrochemical characterization of the cathode suggested that the electrochemical reaction ICl + 2Li → LiI + LiCl is partially reversible in P4VP matrices; its reversibility is mainly limited by the poor chemical stability of P4VP due to the presence of an active hydrogen. Eliminating the active α-H from the polymer structure should greatly improve the stability of the polymer matrices. iCVD polymerization of α-substituted 4-vinylpyridine derivatives should result in polymeric materials resistant to halogenation by ICl or I_2, while retaining desirable properties of charge transfer complex cathodes including sustainability, simple processing, and flexibility. The investigation of these novel polymer chemistries for thin film CTC cathodes is expected to be an important direction for continued research.

Conflicts of interest

The authors declare no conflict of interest.

Acknowledgements

This study is supported by the National Science Foundation under Grant No. 1845805.

References

1. J. F. M. Oudenhoven, R. J. M. Vullers and R. Schaijk, *International Journal of Energy Research*, 2012, **36**, 1139-1150.
2. A. Patil, V. Patil, D. Wook Shin, J.-W. Choi, D.-S. Paik and S.-J. Yoon, *Materials Research Bulletin*, 2008, **43**, 1913-1942.
3. M. E. Donders, W. M. Arnoldbik, H. C. M. Knoops, W. M. M. Kessels and P. H. L. Notten, *Journal of the Electrochemical Society*, 2013, **160**, A3066-A3071.
4. S. Lobe, A. Bauer, S. Uhlenbruck and D. Fattakhova‐Rohlfing, *Advanced Science*, 2021, DOI: 10.1002/advs.202002044, 2002044.
5. Y. Su, J. Falgenhauer, A. Polity, T. Leichtweiß, A. Kronenberger, J. Obel, S. Zhou, D. Schlettwein, J. Janek and B. K. Meyer, *Solid State Ionics*, 2015, **282**, 63-69.
6. E. G. Herbert, W. E. Tenhaeff, N. J. Dudney and G. M. Pharr, *Thin Solid Films*, 2011, **520**, 413-418.
7. M. S. J. Hashmi, *Elsevier*, 2014.
8. M. Koo, K. I. Park, S. H. Lee, M. Suh, D. Y. Jeon, J. W. Choi, K. Kang and K. J. Lee, *Nano Lett*, 2012, **12**, 4810-4816.
9. J. B. Bates, N. J. Dudney, B. J. Neudecker, F. X. Hart, H. P. Jun and S. A. Hackney, *Journal of the Electrochemical Society*, 2000, **147**, 59-70.
10. X. Zhao, Z. Zhao-Karger, M. Fichtner and X. Shen, *Angew Chem Int Ed Engl*, 2020, **59**, 5902-5949.
11. J. B. Goodenough and K. S. Park, *J Am Chem Soc*, 2013, **135**, 1167-1176.
12. J. Heiska, M. Nisula and M. Karppinen, *Journal of Materials Chemistry A*, 2019, **7**, 18735-18758.
13. J. J. Shea and C. Luo, *ACS Appl Mater Interfaces*, 2020, **12**, 5361-5380.
14. M. Nisula and M. Karppinen, *Journal of Materials Chemistry A*, 2018, **6**, 7027-7033.
15. Y.-N. Zhou, M.-Z. Xue and Z.-W. Fu, *Journal of Power Sources*, 2013, **234**, 310-332.
16. K. K. Gleason and P. Baumann, *Weinheim, Germany: Wiley-VCH*, 2015.
17. A. Asatekin, M. C. Barr, H. Baxamusa, K. K. S. Lau, W. E. Tenhaeff, J. P. Xu and K. K. Gleason, *Materials Today*, 2010, **13**, 26-33.
18. S. Aronson, P. Epstein, D. B. Aronson and G. Wieder, *The Journal of Physical Chemistry*, 1982, **86**, 1035-1037.
19. W. Greatbatch, R. Mead and F. Rudolph, *U.S. Patent No. 3957533*, 1976.
20. Z. Meng, H. Tian, S. Zhang, X. Yan, H. Ying, W. He, C. Liang, W. Zhang, X. Hou and W. Q. Han, *ACS Appl Mater Interfaces*, 2018, **10**, 17933-17941.
21. Y. Zhao, L. Wang and H. R. Byon, *Nat Commun*, 2013, **4**, 1896.
22. Y. L. Wang, Q. L. Sun, Q. Q. Zhao, J. S. Cao and S. H. Ye, *Energy & Environmental Science*, 2011, **4**, 3947.
23. F.-C. Liu, W.-M. Liu, M.-H. Zhan, Z.-W. Fu and H. Li, *Energy & Environmental Science*, 2011, **4**, 1261.
24. A. Gero and J. J. Markham, *The Journal of Organic Chemistry*, 1951, **16**, 1835-1838.
25. W. E. Tenhaeff, L. D. McIntosh and K. K. Gleason, *Advanced Functional Materials*, 2010, **20**, 1144-1151.
26. B. B. Peterson, E. M. Andrews, F. Hung and J. C. Flake, *Journal of Power Sources*, 2021, **492**, 229658.
27. Y. Zhao, N. Huo, S. Ye, A. Boromand, A. J. Ouderkirk and W. E. Tenhaeff, *Advanced Optical Materials*, 2021, DOI: 10.1002/adom.202100334, 2100334.
28. H. Xia and L. Lu, *Electrochimica Acta*, 2007, **52**, 7014-7021.
29. C. M. Julien, A. Mauger and O. M. Hussain, *Materials (Basel)*, 2019, **12**.
30. F. Fairbrother, *Nature*, 1947, 87.
31. M. I. Bernal-Uruchurtu§, G. Kerenskaya and K. C. Janda, *International Reviews in Physical Chemistry*, 2009, **28**, 223-265.
32. G. Cavallo, P. Metrangolo, R. Milani, T. Pilati, A. Priimagi, G. Resnati and G. Terraneo, *Chem Rev*, 2016, **116**, 2478-2601.
33. W. B. Person, R. E. Humphrey, W. A. Deskin and A. I. Popov, *Journal of the American Chemical Society*, 1958, **80**, 2049-2053.
34. E. B. Wilson, *Physical Review*, 1934, **45**, 706-714.
35. E. Groppo, M. J. Uddin, O. Zavorotynska, A. Damin, J. G. Vitillo, G. Spoto and A. Zecchina, *The journal of physical Chemistry C*, 2008, **112**, 19493-19500.
36. A. I. Popov and R. H. Rygg, *Journal of the American Chemical Society*, 1957, **79**, 4622-4625.
37. E. W. William, director, *NIST Chemistry WebBook, NIST standard reference database number 69, Eds. P.J. Linstrom and W.G. Mallard, National Institute of Standards and Technology, Gaithersburg MD, 20899, https://doi.org/10.18434/T4D303, (retrieved July 28, 2021).*
38. B. Golec, P. Das, M. Bahou and Y. P. Lee, *J Phys Chem A*, 2013, **117**, 13680-13690.
39. D. Cook, *Canadian Journal of Chemistry*, 1961, **30**, 2009-2024.
40. A. J. Coury and P. T. Cahalan, *Journal of the Electrochemical Society*, 1980, **127**, 2119-2122.
41. M. W. Chase, *Journal of Physical and Chemical Reference Data, Monograph 9*, 1998, 1-1951.
42. G. Patrick, *Garland Science*, 2012.
43. J. Jamnik and J. Maier, *Journal of the Electrochemical Society*, 1999, **146**, 4183-4188.
44. W. Lai and S. M. Haile, *Journal of the American Ceramic Society*, 2005, **88**, 2979-2997.
45. W. Yourey, L. Weinstein and G. G. Amatucci, *Solid State Ionics*, 2011, **204-205**, 80-86.
46. S. Moulay, *Journal of Polymer Engineering*, 2013, **33**, 389-443.
47. D. R. Burgass, P. J. Linstrom and W. G. Mallard, *NIST Chemistry WebBook, NIST standard reference database number 69*.
48. M. Xing, Z. Z. Zhao, Y. J. Zhang, J. W. Zhao, G. L. Cui and J. H. Dai, *Materials Today Energy*, 2020, **18**, 100534.
49. A. J. Bard and L. R. Faulkner, 2001.
50. W. E. Tenhaeff, X. Yu, K. Hong, K. A. Perry and N. J. Dudney, *Journal of the Electrochemical Society*, 2011, **158**, A1143-A1149.
51. M. Yan, Y. Kawamata and P. S. Baran, *Chem Rev*, 2017, **117**, 13230-13319.
52. N. Basescu, Z.-X. Liu, D. Moses, A. J. Heeger, H. Naarmann, N. Theophilou, *Nature*, 1987, **327**, 403-405.
53. D. T. Hallinan, N. P. Balsara, *Annual Review of Materials Research*, 2013, **43**, 503-525.

54. S. Aronson, S. Wilensky, K. Jawitz, H. Teoh, *Polymer*, 1986, **27**, 101-104.